OXFORD

SOT | Society of Toxicology
www.toxsci.oxfordjournals.org

TOXICOLOGICAL SCIENCES, 148(1), 2015, 108–120

doi: 10.1093/toxsci/kfv166
Advance Access Publication Date: July 29, 2015
Research Article

Rosette Nanotubes Alter IgE-Mediated Degranulation in the Rat Basophilic Leukemia (RBL)-2H3 Cell Line

James D. Ede,*,[1] Van A. Ortega,* David Boyle,* Rachel L. Beingessner,† Usha D. Hemraz,† Hicham Fenniri,‡,[2] James L. Stafford,* and Greg G. Goss*,†,[2]

*Department of Biological Sciences, University of Alberta, Edmonton, Alberta, Canada, T6G 2E9; †National Institute for Nanotechnology, 11421 Saskatchewan Drive, Edmonton, Alberta, Canada, T6G 2M9; and ‡Department of Chemical Engineering, 313 Snell Engineering Center, 360 Huntington Avenue, Northeastern University, Boston, Maryland 02115

[1]To whom correspondence should be addressed at Department of Biological Sciences, University of Alberta, Edmonton, Alberta, Canada, T6G 2E9. Fax: 1-780-492-9234. E-mail: ede@ualberta.ca.

[2]These authors contributed equally to this study.

ABSTRACT

In this study, the effects of rosette nanotube (RNT) exposure on immune cell viability and function were investigated *in vitro* using the rat basophilic leukemia (RBL)-2H3 cell line. RBL-2H3 viability was decreased in a dose- and time-dependent manner after lysine-functionalized RNT (K-RNT) exposure. In addition, K-RNTs had a significant effect on RBL-2H3 degranulation. When K-RNT exposure was concurrent with IgE sensitization, 50 and 100 mg l^{-1} K-RNTs elicited a heightened degranulatory response compared with IgE alone. Exposure to 50 and 100 mg l^{-1} K-RNTs also caused degranulation in RBL-2H3 cells not sensitized with IgE (0 ng ml^{-1} IgE). Furthermore, in cells preexposed to K-RNTs for 2 h and subsequently washed, sensitized, and stimulated with IgE, a potentiated degranulatory response was observed. Using confocal laser scanning microscopy and a fluorescein isothiocyanate (FITC)-functionalized RNT construct (termed $FITC^{1}/TBL^{19}$-RNT), we demonstrated a strong and direct affiliation between RNTs and RBL-2H3 cell membranes. We also demonstrated cellular internalization of RNTs after 2 h of exposure. Together, these data demonstrate that RNTs may affiliate with the cellular membrane of RBL-2H3 cells and can be internalized. These interactions can affect viability and alter the ability of these cells to elicit IgE-FcεR mediated degranulation.

Key words: degranulation; nanotoxicology; inflammation; self-assembly; rosette nanotubes

Biologically inspired rosette nanotubes (RNTs) are a self-assembling nanomaterial (NM) formed in solution from a guanine^cytosine (G^C) hybrid motif through a hierarchical, entropically driven process (Fenniri *et al.*, 2001, 2002b; Moralez *et al.*, 2005). The fundamental self-assembling building block of RNTs can be synthesized to feature either 1 (Fig. 1A) or 2 G^C units (Fig. 1D–E). This leads to the formation of hexameric rosettes, which are maintained by either 18- or 36-hydrogen bonds, respectively. The resulting large and substantially hydrophobic supermacrocycles (Fig. 1B) subsequently stack upon one another to form a stable tubular nanostructure (Fig. 1C and 1F–H), which can be up to several 100 μm long.

RNTs hold potential in a variety of biomedical applications including targeted drug delivery, improved vascular implants, tissue engineering, and enhanced orthopedics (Fine *et al.*, 2009; Song *et al.*, 2011; Sun *et al.*, 2012). RNTs are also metal-free, hydrophilic and can be dispersed in polar media, and thus offer advantages for these applications compared with many other engineered NMs (Fenniri *et al.*, 2001, 2002b). Moreover, RNTs have tunable dimensions and can be engineered to express a diverse range of functional groups on their outer surface through covalent functionalization of the G^C molecule (Borzsonyi *et al.*, 2010; Chhabra *et al.*, 2009; Fenniri *et al.*, 2002a; Tikhomirov *et al.*, 2008). This allows for the manipulation of both their physical

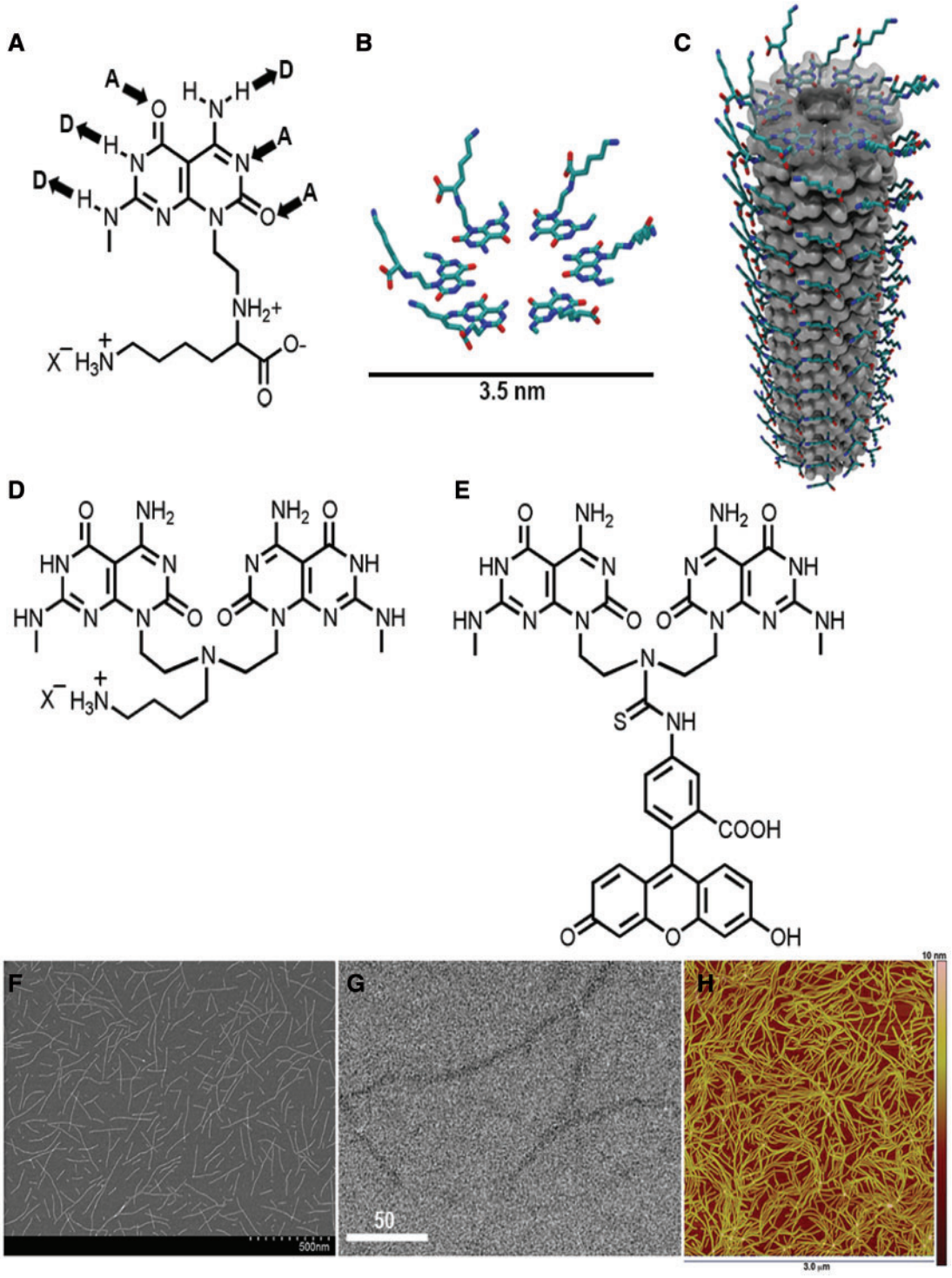

FIG. 1. A, Lysine-functionalized guanine^cytosine (G^C) motif featuring the donor (D) and acceptor (A) hydrogen bonding arrays of guanine and cytosine self-assembles into (B) hexameric rosettes, which further stack to form (C) K-rosette nanotubes (RNTs) having a tubular architecture. Structures of the twin-G^C motifs functionalized with (D) butylamine (termed TB-TBL) and (E) FITC (termed TB-FITC) which were co-assembled to form the FITC[1]/TBL[19]-RNTs. F–H, SEM, TEM, and AFM images of K-RNTs which have an outer diameter of *ca.* 3.5 nm. Scale bar is in nm.

and biological properties (Fenniri *et al.*, 2002a; Fine *et al.*, 2009; Sun *et al.*, 2012). Given the potential utility of RNTs, a thorough assessment of their potential interaction with cells, tissues, and systems is necessary.

A critical factor to consider when assessing the biocompatibility and toxicity of new materials are their interactions with various *in vivo* processes such as those facilitated by the immune system (Remes and Williams, 1992). Recent data has demonstrated that NMs may adversely influence immune cell responses *in vivo* during inadvertent exposure and following deliberate pulmonary, subcutaneous, intraperitoneal, and intravenous introduction (Chen *et al.*, 2010; Kolosnjaj-Tabi *et al.*, 2010;

Meng *et al.*, 2011; Song *et al.*, 2009; Gustafsson *et al.*, 2011). For example, fullerenes have been demonstrated to act as potent antigens, stimulating the production of fullerene-specific IgG antibodies, but have also been shown to be immunosuppressive, suppressing the inflammatory response of peripheral blood basophils and mast cells by inhibiting the activation of signaling intermediates required for exocytosis of immunogenic mediators (Braden *et al.*, 2000; Chen *et al.*, 1998; Ryan *et al.*, 2007). In addition, even subtle changes in NM structure can alter their biological effects; for example, changing the density of functionalized polymers on NMs can switch the complement pathways that are activated upon NM exposure in human serum (Hamad *et al.*, 2010; Sim and Wallis, 2011).

It is important to understand the response of immune cells occupying "sentinel locations" within tissues and at interfaces between the body and environment. Myeloid cells (ie, macrophages and granulocytes) are found throughout body tissues including respiratory, intestinal, and mucosal epithelia and are one of the first activators of the inflammatory response (Passante and Frankish, 2009). Granulocytes (ie, neutrophils and mast cells) contain granules in their cytoplasm, which when stimulated are released via a process called degranulation and include various mediators of immunity. In this study, we investigate the cellular response of rat basophilic leukemia (RBL)-2H3 cells, a granulocyte cell line used extensively in studies of allergy and inflammation, to understand the impact of K-RNT exposure. RBL-2H3 cells express an endogenous, high affinity Fcε receptor (FcεRI), which when bound by IgE in a process called sensitization and subsequently cross-linked by dinitrophenyl-human serum albumin (DNP-HSA), induces degranulation (Gilfillan and Tkaczyk, 2006). Degranulation releases a variety of chemical mediators including histamine, serotonin, and β-hexosaminidase providing a sensitive endpoint to examine the effects of K-RNT exposure on immune effector functions (Huang *et al.*, 2009).

Herein, we examined the influence of K-RNT exposure on RBL-2H3 viability and using the IgE-DNP model, assess the direct effects of RNT exposure on IgE/FcεRI-mediated degranulation to determine if they alter the activation of innate immune responses. As well, using a reporter array, we examined various cell signaling pathways related to cellular toxicity to elucidate the cellular mechanisms that mediate cell death reported here and in previous studies. Finally, confocal microscopy studies were performed to gain insight into the physical interactions between RBL-2H3 cells and RNTs. For this purpose, a RNT termed FITC^{1}/TBL^{19}-RNT, was synthesized through a co-assembly process of TB-FITC (Fig. 1D) and twin based-butylamine (TB-TBL) (Fig. 1E) in a 1:19 molar ratio, to express the fluorescent marker fluorescein isothiocyanate (FITC), while maintaining a solubility and surface charge profile similar to K-RNTs (Fenniri *et al.*, 2001).

MATERIALS AND METHODS

RNT synthesis and characterization. The synthesis of the lysine functionalized G^C motif (Fig. 1A) and self-assembly into a stock solution of K-RNTs (1 g l^{-1}) (Fig. 1C) in nanopure water was performed and extensively characterized according to a previously reported procedure (Fenniri *et al.*, 2001, 2002b). The synthesis of TB-TBL (Fig. 1D) has also been previously reported, while the preparation of TB-FITC (Fig. 1E) will be described in due course. For the preparation of the stock solution of co-assembled FITC^{1}/TBL^{19}-RNTs (1:19 molar ratio, 385 mg l^{-1} total), a solution of TB-TBL in nanopure water was sonicated for 30 s and then transferred to a vial containing TB-FITC. The suspension was sonicated for 5 min, vortexed for 5 s, followed by heating using a heat gun (on high setting) for 1 min. This procedure was repeated twice or until no further dissolution occurred. The yellow suspension was allowed to stand at room temperature in the dark for 2 days to allow for the growth of the RNTs and sedimentation of any undissolved TB-FITC. The yellow supernatant was then transferred into another glass vial and was stored in the fridge in the dark. Aliquots from this stock solution of FITC^{1}/TBL^{19}-RNTs were diluted and used for the cell studies.

The hydrodynamic diameter and zeta-potentials of K-RNTs and FITC^{1}/TBL^{19}-RNTs at concentrations of 1, 10, 50 mg l^{-1} and 10, 50 mg l^{-1}, respectively, were determined using dynamic light scattering (DLS; Malvern Instrument Zetasizer Nano ZS, Westborough, Massachusetts). Hydrodynamic radii were measured using 173° backscattering mode and reported as the peak value of > 99% intensity. Extensive characterization details of RNTs under a variety of physiological conditions and with various side-group functionalizations have been previously reported and the reader is directed to previous studies by Fenniri *et al.* (2001, 2002a) and Moralez *et al.* (2005) for full details. However, a summary profile with pertinent information for this study has been included as Supplementary Table S1.

Cell culture. RBL-2H3 cells were cultured at 37°C and 5% CO_2 in filter sterilized (0.22 μm, Corning) Minimum Essential Media (MEM; Hyclone) containing 10% heat-inactivated fetal bovine serum (FBS) (characterized; Hyclone) supplemented with 2mM L-glutamine (Gibco), 100 units ml^{-1} penicillin (Gibco), and 100 μg ml^{-1} streptomycin (Gibco) as described previously (Cortes *et al.*, 2014).

Human embryonic kidney (HEK) 293T cells were cultured at 37°C and 5% CO_2 in filter sterilized (0.22 μm, Corning) DMEM/High glucose (Hyclone) containing 10% heat-inactivated FBS (characterized; Hyclone) supplemented with 2mM L-glutamine (Gibco), 100 units ml^{-1} penicillin (Gibco), 100 μg ml^{-1} streptomycin (Gibco), 1mM sodium pyruvate (Gibco), and 1% MEM non-essential amino acid solution (Gibco).

Examination of RBL-2H3 and HEK 293T viability following exposure to K-RNTs. RBL-2H3 cells were seeded in a 96-well plate at a density of 40 000 cells per well and allowed to attach for 1 h (37°C, 5% CO_2) before dosing with 1, 10, 50, 100, or 200 mg l^{-1} K-RNT in MEM for 2, 4, or 24 h (37°C, 5% CO_2). We recognize that several dosing metrics have been identified for NMs and provide the conversions between mass per volume, particles per volume and surface area per volume in Supplementary Table S2. Control wells received MEM alone (negative control) or 40 μl of nanopure water (vehicle control). Following exposure, cells were harvested, washed twice with ×1 PBS, and resuspended in 200 μl of ×1 PBS/propidium iodide (PI) (100 μg ml^{-1}) and analyzed by flow cytometry (Quanta SC, Beckman Coulter). Whole cell populations were gated using side scatter and forward scatter. An increase in PI fluorescence, indicative of cell death, was detected using the FL2 filter. The percentage of viable cells in culture was calculated from the number of cells within the whole population gate that concurrently exhibited low levels of PI fluorescence. Viability is expressed relative to negative controls, calculated as a percentage of viable RNT-exposed cells to viable unexposed cells.

The effects of RNTs on cell viability were also studied using a nonradioactive cell proliferation assay performed according to the manufacturer's instructions (Cell Titer 96 Aqueous NonRadioactive Cell Proliferation Assay Kit, Promega,

Wisconsin). MTS [3-(4,5-dimethylthiazol-2-yl)-5-(3-carboxymethoxyphenyl)-2-(4-sulfophenyl)-2H-tetrazolium] when bioreduced by cells can gauge cell number by recording a change in absorbance at 490 nm. RBL-2H3 cells were seeded in a 96-well plate at a density of 40 000 cells per well and allowed to attach for 1 h (37°C, 5% CO_2) before dosing with 1, 10, 50, 100, or 200 mg l^{-1} K-RNT in MEM for 2, 4, or 24 h (37°C, 5% CO_2). HEK-293T cells were seeded in a 96-well plate at a density of 25 000 cells per well. Cells were allowed to attach for 2 h before exposing them to 0.5, 1, 5, 10, 50, or 100 mg l^{-1} K-RNT in DMEM for 6 h (37°C, 5% CO_2), which was the exposure time used for the luciferase reporter assay (see section 2.4 later). Following the exposures, RBL-2H3 or HEK-293T cells were washed with complete media (MEM or DMEM, respectively) and prepared kit reagents were added to the plate for an additional 1 h (37°C, 5% CO_2). Absorbance at 490 nm was then measured using a microplate reader (WALLAC 1420, PerkinElmer, Massachusetts). Previous studies have demonstrated that RNTs can interfere with colorimetric assays, including the MTS assay despite the inclusion of several wash steps (Ong *et al.*, 2014). The UV/Vis (ultraviolet/visible) absorption spectra of K-RNTs is provided as Supplemental Figure S1. Pairwise controls containing cells exposed to K-RNTs were used to control for absorbance caused by RNTs alone. Viability was calculated based on the following formula:

Viability (% Control) = (Abs of RNT treated cells – Abs of RNT control)/(Abs of negative control – Abs of background control)

Effects of K-RNT exposure on intracellular toxicity-related signaling pathways. To investigate the intracellular signaling events underlying the toxicity observed at higher doses of K-RNTs, highly transfectable human embryonic kidney (HEK)-293T cells were employed and a transfected reporter array was used to identify changes in 10 broad intracellular toxicity-related signaling pathways using Cignal Finder Toxicity 10-Pathway Reporter Array (SABiosciences). This luciferase-based reporter measures changes in intracellular signaling of 10 toxicity-related signaling pathways: (1) p53/DNA damage, (2) hypoxia, (3) NFκβ, (4) glucocorticoid receptor, (5) cell cycle/pRB-E2F, (6) MAPK/ERK (mitogen activated protein kinases/extracellular signal-related kinases), (7) MAPK/JNK (mitogen activated protein kinases/c-Jun N-terminal kinases), (8) (protein kinase C) PKC/Ca^{2+} (9) TGFβ, and (10) Myc/Max. Each reporter also consists of a constitutively expressing *Renilla* construct allowing for transfection efficiencies to be normalized. In addition, the kit includes a negative control (noninducible reporter) and a positive control (constitutively expressing both firefly luciferase and a green fluorescent protein (GFP) construct).

Transfections were performed according to the manufacturer's instructions using HEK-293T cells seeded in a 96-well plate. Cells were seeded at a density of 25 000 cells/well in 200 µl complete DMEM and incubated overnight (37°C and 5% CO_2). Cells were then transfected with 100 ng of Cignal Reporter Constructs. For all 12 Cignal Reporters, a master mix was created consisting of 400 ng of Cignal Reporter, 20 µl of OptiMEM (Invitrogen) and 0.4 µl of Turbofect (Fermentas) per well. This solution was gently mixed and allowed to sit at room temperature for 15 min. Next, 21 µl of master mix was added to each well and the cells were incubated for 24 h (37°C and 5% CO_2) at which time, the media was removed and cells were exposed to 50 or 100 mg/l K-RNT in complete DMEM for 6 h (37°C and 5% CO_2). Cells were then washed and assayed for firefly and *Renilla* luciferase activity using Dual-Glo Luciferase Assay System (Promega).

A ratio of luminescence from the experimental reporter (firefly luminescence) to the control reporter (*Renilla* luminescence) was used to control for transfection efficiency. A quotient of the firefly:*Renilla* ratio for cells treated with K-RNTs (firefly:$Renilla^{txt}$) to the firefly:*Renilla* ratio for control treatments (firefly:$Renilla^{ctrl}$) was calculated and represents a change in luminescence for RNT exposure compared with control.

Examination of RBL-2H3 degranulation in the presence of K-RNTs. RBL-2H3 degranulation was measured using the β-hexosaminidase release assay as described previously (Cortes *et al.*, 2012). Briefly, RBL-2H3 cells were seeded into a flat bottom 96-well plate (Costar) at a density of 40 000 cells per well and allowed to attach for 2 h in complete MEM (37°C, 5% CO_2). Next, cells were sensitized with 0, 12.5, 25, 50, or 100 ng ml^{-1} of mouse anti-DNP IgE mAb (Sigma-Aldrich) in incomplete Tyrodes buffer (25mM 4-(2-hydroxyethyl)-1-piperazineethanesulfonic acid (HEPES), 140mM NaCl, 1.8mM $CaCl_2$, 5.6mM D-glucose, 12mM $NaHCO_3$, 0.37mM NaH_2PO_4, and $MgCl_2$, pH 7.4) for 1 h at 37°C and 5% CO_2. Solutions were then removed and the cells washed with 200 µl of Tyrodes buffer containing 0.1% bovine serum albumin (BSA). Cells were then stimulated to degranulate with 0.05 µg ml^{-1} DNP-HSA in Tyrodes/BSA buffer heated to 37°C. Negative controls were exposed to Tyrodes buffer alone to measure nonspecific background signal. The efficacy of the assay was verified by use of a positive control, 0.625 µM calcium ionophore A23187 (Sigma-Aldrich). Cells were placed in the incubator for 1 h at 37°C and 5% CO_2 and the amount of β-hexosaminidase released by RBL-2H3 cells was then assayed by removing 25 µl of the supernatant and combining it with 100 µl of β-hexosaminidase substrate buffer (2mM 4-methylumbelliferyl N-acetyl-b-D-glucosaminide (Sigma–Aldrich), 100mM citrate, pH 4.5) for 30 min at 37°C and 5% CO_2. The wash steps and sampling of the supernatant limited the concentration of RNTs present in the final assay components, eliminating potential interference of RNTs with this assay. The reaction was quenched by adding 150 µl of 200mM L-glycine, pH 10.7. The cleavage of the substrate 4-methylumbelliferyl N-acetyl-b-D-glucosaminide by β-hexosaminidase was measured using a microplate reader with 360 nm excitation and 450 nm emission filters (WALLAC 1420, PerkinElmer). The relative fluorescence units (RFUs) for the treatments were standardized to our negative control (nonspecific background).

Using the earlier protocol, 2 experimental approaches were devised to investigate different mechanisms by which K-RNTs may affect the degranulatory response of RBL-2H3 cells. The first experiment examined if preexposing RBL-2H3 cells to K-RNTs affected degranulation when subsequently sensitized and stimulated, thereby examining if K-RNTs exposure could affect the long-term function of immune cells to elicit the appropriate immunological responses. Here, cells were first exposed to 50 or 100 mg l^{-1} K-RNT solutions in complete MEM for 2 h (37°C, 5% CO_2) and washed thrice with complete Tyrodes buffer prior to sensitization with IgE. Cells were then stimulated and degranulation was assessed. Control treatments consisted of a 2 h exposure to the ultra pure water vehicle.

In the second experiment, cells were co-exposed to either 50 or 100 mg l^{-1} K-RNTs and IgE to examine if the presence of K-RNTs interferes with IgE binding FcεRI during sensitization, a step required to elicit IgE/FcεRI-mediated degranulation in RBL-2H3 cells. Here, during sensitization with 0, 12.5, 25, 50, or 100 ng ml^{-1} IgE, cells were simultaneously exposed to 50 and 100 mg l^{-1} K-RNT for 1 h at 37°C and 5% CO_2. Solutions were then removed and the cells were washed with 200 µl of complete Tyrodes buffer and the protocol was followed as described above. Control treatments consisted of a simultaneous vehicle (ultrapure water) and IgE exposure.

TABLE 1. Physicochemical Characterization of K- and FITC[1]/TBL[19]-RNTs Showing Hydrodynamic Diameter (nm) and Zeta Potential (mV) Diluted to 1, 10, and 50 mg l^{-1} in Ultra Pure H_2O Reported as Mean ± SD.

Material	Concentration (mg l^{-1})	Hydrodynamic Diameter (nm)	Polydispersity	Zeta Potential (mV)
K-RNT	1	280 ± 169	0.41 ± 0.12	
	10	397 ± 136	0.34 ± 0.08	71 ± 3
	50	405 ± 122	0.31 ± 0.05	72 ± 2
FITC1/TBL19 -RNT	10	312 ± 133	0.38 ± 0.07	17 ± 2

Examination of FITC[1]/TBL[19]-RNT interaction with RBL-2H3 cells by confocal microscopy. FITC[1]/TBL[19]-RNTs were used to investigate the cellular association of RNTs with RBL-2H3 cells. Glass coverslips (Fisher Scientific) were treated with 70% ethanol, washed with ×1 PBS and subsequently UV-irradiated. RBL-2H3 cells were seeded on coverslips in a 6-well plate at a density of 1×10^5 and allowed to grow for 48 h (37°C, 5% CO_2). After incubation, cells were exposed to 10 mg l^{-1} FITC[1]/TBL[19]-RNTs for 2, 4, or 6 h. Cells were washed with antibody staining buffer (phosphate buffered saline, 0.5% bovine serum albumin) antibody staining buffer (ASB). Coverslips were then placed on parafilm containing ASB with 100 ng ml^{-1} IgE mAb for 30 min over ice. Cells were washed with ASB and then placed on parafilm containing ASB with 50 ng ml^{-1} goat anti-mouse IgG R-phycoerythrin (PE)-conjugated staining antibody (Beckman Coulter) at 4°C for 30 min in the dark. Cells were subsequently washed with ASB before being placed in Fixation Buffer (BioLegend) for 20 min at room temperature in the dark. Finally, cells were washed with ASB and mounted on slides using mounting media containing 4′,6-diamidino-2-phenylindole (DAPI). Slides were viewed with a Laser Scanning Confocal Microscope (Zeiss LSM 710, objective 40 × 1.3 oil plan-Apochromat) at the Cross Cancer Institute Cell Imaging Facility, Edmonton, Alberta. Images were collected with Zen (2011) software and processed with LSM Image Browser (v. 4.2.0.121, Carl Zeiss). Surface rendering and 3-dimensional (3D) reconstruction of Z-stack images were performed using Imaris software (v. 6.2.2, Bitplane).

Statistical analysis. To investigate the effect of RNT exposure on RBL-2H3 viability, 2-way Analysis of Variance (ANOVA) followed by *post hoc* Bonferroni test were performed. To determine the effect of RNT exposure on RBL-2H3 degranulation, 2-way ANOVA were performed to determine differences between experimental and control treatments followed by *post hoc* Sidak's test. To investigate the effect of RNT exposure on HEK 293T viability, a 1-way ANOVA followed by *post hoc* Dunnett's test were performed. All statistical analyses were performed using GraphPad 6.0 statistical software program. Statistical significance was set at $p < .05$; n refers to the number of independent experiments conducted on cultured cells.

RESULTS

Sample Characterization

For this study, K-RNTs self-assembled from the lysine-functionalized G^C motif were characterized as previously described (Fenniri *et al.*, 2001). Representative scanning electron microscopy (SEM), transmission electron microscopy (TEM), and atomic force microscopy (AFM) images of the nanotubes are shown in Figure 1F–1H, which have an average outer diameter of *ca.* 3.5 nm (Fenniri *et al.*, 2001). DLS measurements shown in Table 1 revealed that the hydrodynamic radii of K-RNTs at concentrations of 10 and 50 mg l^{-1} in ultra pure water were (mean ± SD, $n = 4$) 397 ± 136 and 405 ± 122 nm, respectively. The measured ζ-potential of K-RNTs at 10 mg l^{-1} was 71 ± 3 mV and this value did not change at a higher concentration of 50 mg l^{-1} (72 ± 2 mV). Unfortunately, it was not possible to characterize RNTs in cell culture media using currently available common techniques such as DLS because the concentrations tested in this complex matrix were below the instruments detection limit. To give the reader additional RNT characterization, Supplementary Table S1 summarizes data from several publications. In our analysis, we use gravimetric measures as an indicator of dose. Because these high aspect ratio RNT materials do not increase in either individual diameter or length with increasing dose, both surface area and molarity will increase linearly with gravimetric dose. The conversion factors for recalculation of dose as either surface area or molarity are provided in Supplemental Table S2.

Effects of RNTs on RBL-2H3 Viability

Exposure to K-RNTs resulted in a significant change in adherent RBL-2H3 viability, with both dose- and time-dependent effects observed. Flow cytometric analysis revealed no significant change in viability for 2, 4, or 24 h exposure to 1, 10, and 50 mg l^{-1} K-RNT (Fig. 2A). However, while exposure to 100 mg l^{-1} K-RNT for 2 and 4 h did not result in a significant change in viability, there was a significantly decreased viability after 24 h of exposure (mean ± S.E.M., $n = 4$; 84.37 ± 1.64%) compared with control (Fig. 2A). At 200 mg l^{-1} effects of K-RNTs appeared earlier during the exposure with viability significantly decreased to: 81.4 ± 2.6, 83.1 ± 2.7, and 74.8 ± 2.6% of control at 2, 4, and 24 h, respectively (Fig. 2A).

Results using the MTS assay to measure cell proliferation and verify viability results demonstrated that exposure to K-RNTs caused a significant decline in cell viability that was both dose- and time dependent (Fig. 2B). Similar to the flow cytometric viability analysis (Fig. 2A), there was no significant change in RBL-2H3 viability after 2, 4, or 24 h at exposure levels of 1, 10, or 50 mg l^{-1} K-RNT. However, 100 mg l^{-1} of K-RNT after 2, 4, and 24 h resulted in significant declines in viability, compared with controls. Cells exposed to 100 mg l^{-1} had viability significantly decreased to (mean ± S.E.M., $n = 8$): 82.2 ± 1.7, 76.5 ± 6.2, and 75.4 ± 7.1% of control after 2, 4, and 24 h, respectively (Fig. 2B). Exposure to 200 mg l^{-1} K-RNT further reduced RBL-2H3 viability at 4 and 24 h with 67.2 ± 5.4%, and 66.3 ± 7.5% viability compared with controls (Fig. 2B).

Characterizing Changes in Intracellular Signaling Toxicity-Related Pathways Upon K-RNT Exposure

We sought to investigate the intracellular signaling events underlying the toxicity observed at higher doses of K-RNTs (Fig. 3). To accomplish this, HEK-293T cells were transfected with a series of luciferase-based reporters, each specific for monitoring the transcriptional activity of 10 intracellular signaling pathways related

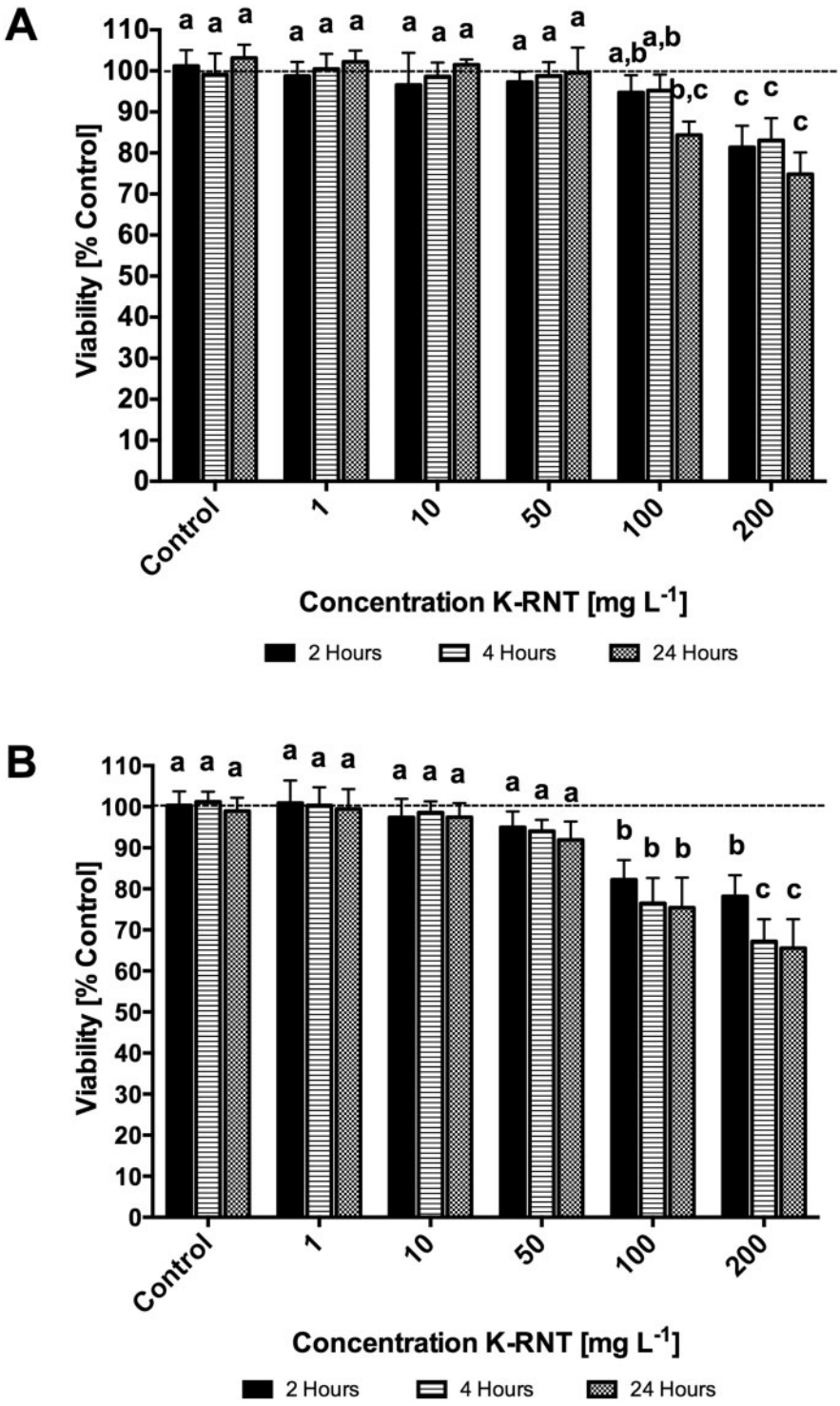

FIG. 2. Exposure to K-RNTs significantly affected rat basophilic leukemia (RBL)-2H3 viability. A, 4×10^4 RBL 2H3 cells were exposed to 1, 10, 50, 100, or 200 mg l^{-1} K-RNT for 2, 4, or 24 h. Cells were stained using propidium iodide (100 μg ml^{-1}) and analyzed by flow cytometry using FL2 to distinguish between viable and nonviable cells. Viability is expressed relative to negative controls, calculated as a percentage of viable RNT-exposed cells to viable unexposed cells. Values are means ± SE ($n = 4$) (B) 4×10^4 RBL-2H3 cells were exposed to 1, 10, 50, 100, or 200 mg l^{-1} K-RNT for 2, 4, or 24 h. Metabolic activity, as an indicator of cell viability, was measured in cells after exposure using the MTS assay. Absorbance values were measured at 490 nm and compared with control to calculate percent cell viability. Values are means ± SE ($n = 8$). Letters indicates significantly different values ($p < .05$, 2-way ANOVA followed by Bonferroni *post hoc* comparison).

to toxicity. During assay optimization, the greatest changes in transcriptional activity were measured after 6 h exposure to the positive control, cadmium selenide nanoparticles (Supplementary Fig. S2). First, we verified that the viability of HEK-293T exposed to K-RNTs for 6 h was similar to that observed for RBL-2H3 cells. HEK-293T cells showed a decrease in viability upon exposure to K-RNTs at doses of 50 (mean ± S.E.M., $n = 5$; 89 ± 2.9%) and 100 mg l^{-1} (72 ± 2.31%) (Fig. 3A). Examination of the luciferase activity

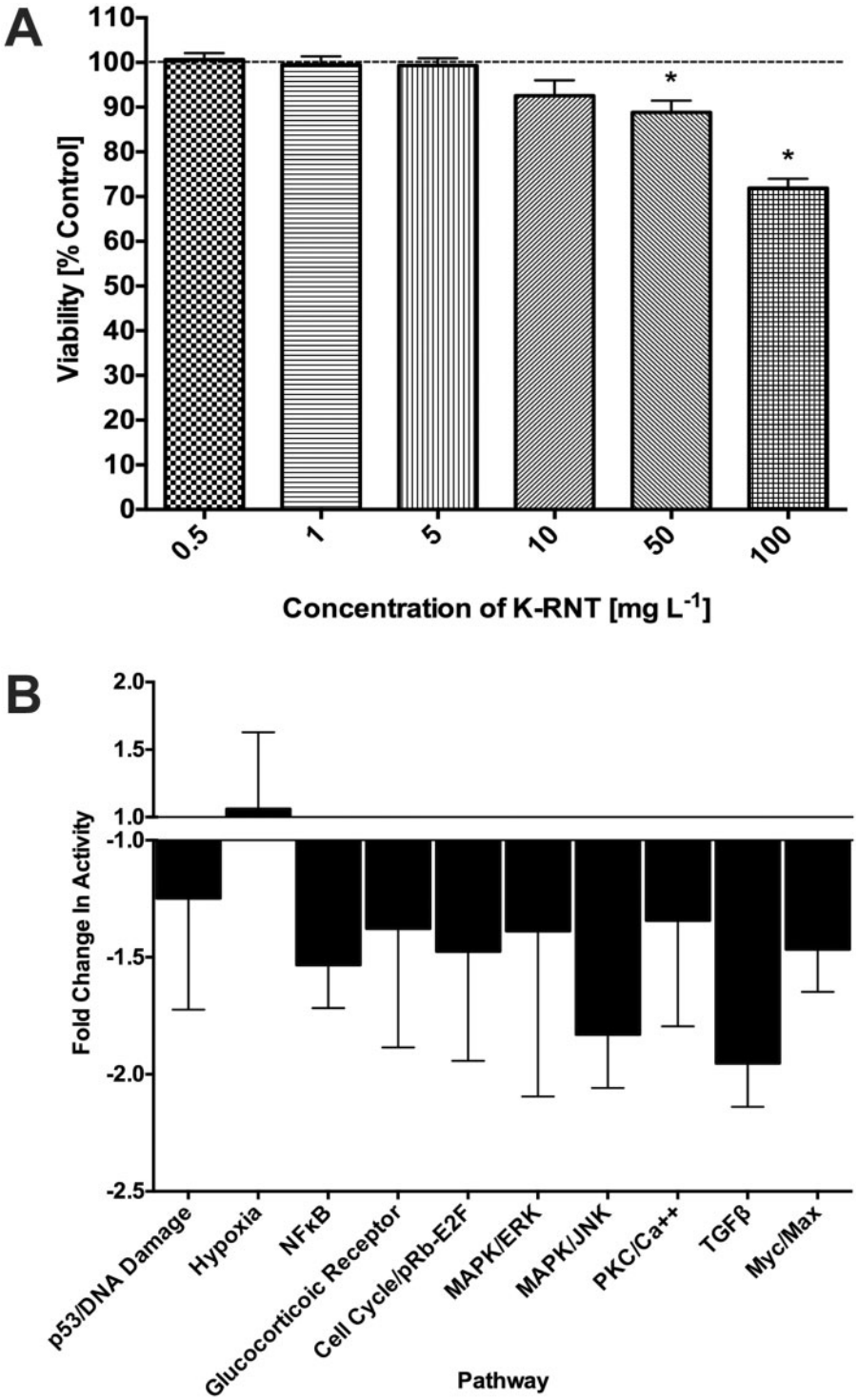

FIG. 3. Exposure to K-RNTs did not change the transcriptional activity of 10 toxicity-related signaling pathways in HEK 293T cells. A, 2.5×10^4 HEK 293T cells were exposed to 0.5, 1, 5, 10, 50, or 100 mg l^{-1} K-RNT for 6 h. Metabolic activity, as an indicator of cell viability, was measured in cells after exposure using the MTS assay. Absorbance values were measured at 490 nm and compared with control to calculate percent cell viability. Values are means ± SE ($n = 8$). Letters indicates significantly different values ($p < .05$, 1-way ANOVA followed by Dunnett's *post hoc* comparison). B, 2.5×10^4 HEK 293T cells were transfected with 1 of 10 Cignal Reporter Constructs for 24 h. Constructs represent a luciferase reporter gene linked to a specific transcriptional response element for 10 broad, intracellular toxicity-related signaling pathways. Cells were exposed to 50 mg l^{-1} K-RNT in growth media for 6 h. Cells were then assayed for luciferase activity as an indicator of intracellular signaling activation. K-RNT treatment is standardized to vehicle control treatment and is expressed as fold-change in luminescence activity. Asterisk indicates significantly different values compared with control ($n = 5$, $p < .05$, 1-way ANOVA followed by Dunnett's *post hoc* comparison).

after 6 h exposure to 50 mg l^{-1} K-RNT revealed a general downregulation of multiple toxicity-related pathways with the exception of hypoxia inducible factor, which remained unchanged (Fig. 3B). Luciferase activity after 3 and 12 h RNT exposure showed a similar trend (Supplementary Fig. S2).

Degranulation of RBL-2H3 Cells in Response to RNT Exposure

In the first series of experiments, RBL-2H3 cells were simultaneously sensitized with 0, 12.5, 25, 50, or 100 ng ml^{-1} IgE and exposed to 50 or 100 mg l^{-1} K-RNTs. In all treatments tested, there was an increase in the degranulatory response of the cells (Fig. 4A–4C). This effect was observed irrespective of the concentration of IgE (12.5, 25, 50, or 100 ng ml^{-1}) or concentration of K-RNT (50 or 100 mg l^{-1}) tested (Fig. 4A and 4B). The presence of K-RNTs at either 50 or 100 mg l^{-1} resulted in an increased degranulatory response, ranging from (mean ± S.E.M., $n = 5$) 119 ± 3.9% to 140 ± 7.2% of controls (Fig. 4C). It should be noted that when IgE was not present (0 ng ml^{-1}), exposure to either 50 or 100 mg l^{-1} K-RNT still resulted in a significantly elevated β-hexosaminidase release (126.6 ± 3.9% and 120 ± 3.8%, respectively).

The second experiment examined if preexposure to either 50 or 100 mg l^{-1} of K-RNTs for 2 h affects the ability of RBL-2H3 cells to degranulate when subsequently washed, sensitized, and stimulated. Preexposure to 50 mg l^{-1} of K-RNT showed a potentiated degranulatory response starting at higher doses of IgE (25 mg l^{-1} and above), relative to controls (Fig. 5A). Cells preexposed to 100 mg l^{-1} of K-RNT for 2 h displayed a potentiated degranulatory response at all concentrations of IgE tested ((mean ± S.E.M., $n = 5$) 12.5 ng ml^{-1}: 123 ± 4.3%; 25 ng ml^{-1}: 129 ± 3.6%; 50 ng ml^{-1}: 126 ± 1.6%; and 100 ng ml^{-1}: 123 ± 1.5%) (Fig. 5B). Of note, cells that were preexposed to 50 and 100 mg l^{-1} K-RNT but were not sensitized with IgE (0 ηg ml^{-1} IgE) did not have an elevated degranulatory response (Fig. 5C). This contrasts with the previous experiment when K-RNT and IgE were exposed simultaneously during sensitization (Figs. 4C and 5C).

Examination of FITC^1/TBL^{19}-RNT Interaction With RBL-2H3 Cells by Confocal Microscopy

Confocal laser scanning microscopy of FITC^1/TBL^{19}-RNTs demonstrated that RNTs bind to RBL-2H3 cells. When RBL-2H3 cells were exposed to 10 mg l^{-1} FITC^1/TBL^{19}-RNTs for 4 or 6 h, extensive co-localization between RNTs and FcεR was observed (Fig. 6). Micrographs showing DAPI fluorescence (Fig. 6A–6C), FcεR fluorescence (Fig. 6D–6F), and FITC^1/TBL^{19}-RNT fluorescence (Fig. 6G–6I) suggest that FITC-RNTs are associated with FcεR as demonstrated through co-localized fluorescence (Fig. 6J–6O). This association remained despite the extensive washing of RBL-2H3 cells during confocal preparation, suggesting a strong affiliation between the two.

Using the fluorescence of DAPI, a nuclear stain, as a reference point for the intracellular compartment, FITC^1/TBL^{19}-RNT fluorescence is observed within the cell interior, visualized through 3D reconstruction of Z-stack images (Fig. 6P and 6Q). This suggests FITC^1/TBL^{19}-RNTs can be internalized by RBL-2H3 cells after just 2 h of exposure.

Discussion

Effects of K-RNT on Immune Cell Viability

Cell viability was assessed through a combination of flow cytometric analysis and the MTS assay. RBL-2H3 cells showed a dose dependent decrease in cell viability with increasing doses of K-RNTs after 2 and 4 h of exposure with significant decreases in metabolic activity at 100 and 200 mg l^{-1} K-RNT. By comparison, Journeay *et al.* (2008) demonstrated a significant reduction in the viability of the pulmonary epithelial cell line Calu-3 after a 24 h exposure to 50 mg l^{-1} K-RNTs. Similarly, a human macrophage cell line, U937, demonstrated a significant decrease in viability after 24 h exposure to 50 mg l^{-1} K-RNTs (Journeay *et al.*, 2009). Although a significant change in RBL-2H3 cell viability at 50 mg l^{-1} K-RNT was not observed, the epithelial cell line HEK 293T did exhibit a significant decrease in cell viability after 6 h of exposure to 50 and 100 mg l^{-1} K-RNTs. Differential susceptibility of several cell lines has been reported in studies on metal toxicity (Tan *et al.*, 2008). Pfaller *et al.* (2009) in their investigation of immunomodulatory effects of NMs noted significant differences in sensitivity of A549, Jurkat, and THP-1 cell lines. Our results, together with previous findings, highlight the need to use a variety of models and viability assays when investigating the biocompatibility of new materials (Zhao *et al.*, 2013).

With demonstrated changes in viability upon K-RNT exposure, an investigation into the mechanisms of observed cell death was warranted. The use of a luciferase-based reporter system has been used with success to survey a broad list of potential mechanisms of zinc oxide and platinum nanoparticle toxicity for further study (Rallo *et al.*, 2011). In general, it was found that after 6 h of K-RNT exposure, the transcriptional activity related to a broad variety of intracellular signaling pathways was downregulated with the exception of hypoxia inducible factor, which remained unchanged. However, no significant changes in transcriptional activity were observed. Many of these candidate signaling pathways play important roles in apoptosis including PKC/Ca^{2+}, Myc/Max and p53/DNA damage. The lack of induction of these pro-apoptotic pathways by K-RNT exposure suggests the possibility of nonapoptotic mechanisms of cell death such as regulated or unregulated necrosis (Sun and Wang, 2014).

Using FITC^1/TBL^{19}-RNTs, the cellular association and subsequent internalization of the nanotubes in RBL-2H3 cells was confirmed. This is the first demonstration of the cellular uptake of RNTs using confocal imaging. Confocal micrographs show co-localization between IgE labeled FcεR and FITC^1/TBL^{19}-RNTs, suggesting these NMs are associating with the cellular membrane. The presence of FITC^1/TBL^{19}-RNTs, despite extensive washing, demonstrates a strong association between this material and the cell membrane surface receptors. In computer simulations, functionalizing gold NMs with positive surface charges resulted in increased lipid bilayer adherence when compared with negative and hydrophobic surface functionalizations (Lin *et al.*, 2010). It is likely that the high level of FITC^1/TBL^{19}-RNT and cell membrane interaction results from the attraction between the positively charged nanotubes (Table 1) and negatively charged cell membranes. 3D reconstruction and surface renderings of Z-stacks also suggest the internalization of FITC^1/TBL^{19}-RNTs after 2 h exposure. Such strong affiliation of RNTs with the membrane could potentially contribute to a loss of membrane integrity, causing cell death through a nonregulated necrotic process. With a lack of candidates identified from the reporter assay, our lab is currently investigating if necrosis could be the mechanism of RNT toxicity observed at higher doses.

Effects of K-RNT on RBL-2H3 Cell Degranulation

Endpoints beyond viability are being recognized as important in the toxicological evaluation of NMs (Ortega *et al.*, 2013). Here, we demonstrate for the first time an immediate degranulatory event by RBL-2H3 cells when exposed to K-RNTs. Interestingly,

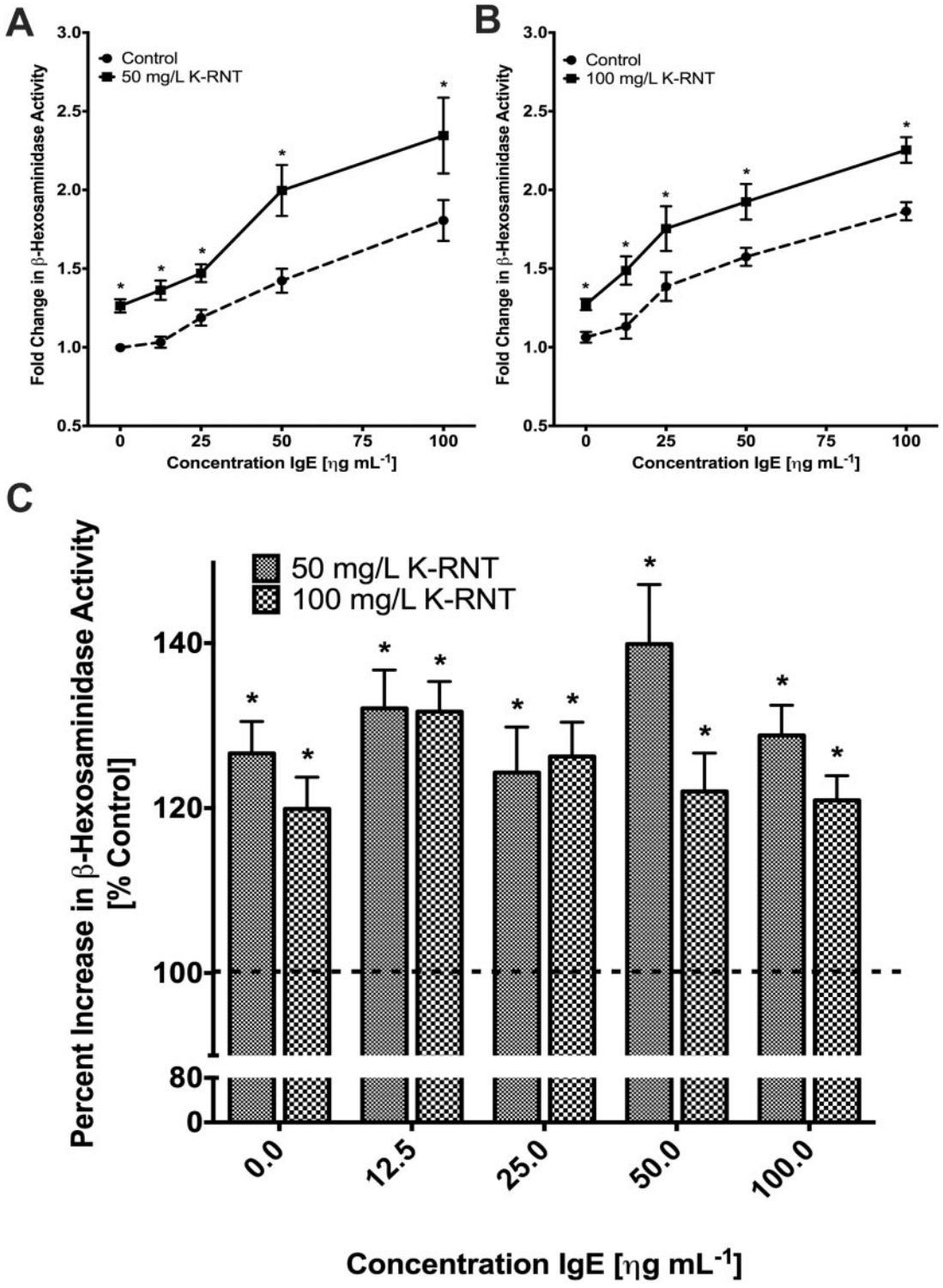

FIG. 4. RBL-2H3 cells increased release of β-hexosaminidase when co-exposed to K-RNTs during IgE sensitization. RBL-2H3 cells were seeded at 4×10^4 into a 96-well plate and allowed to rest for 2 h. Cells were simultaneously sensitized with IgE (0, 12.5, 25, 50, or 100 ng ml^{-1}) and exposed to either (A) 50 or (B) 100 mg l^{-1} K-RNT. Control cells were simultaneously sensitized with IgE (0, 12.5, 25, 50, or 100 ng ml^{-1}) and exposed to vehicle (ultra pure H_2O). Negative controls were exposed to Tyrodes buffer alone (no IgE) to measure nonspecific background signal. After washing, cells were subsequently stimulated to degranulate with dinitrophenyl-human serum albumin (DNP-HSA). Supernatant was collected and β-hexosaminidase activity assayed. The relative fluorescent units (RFUs) for each treatment was standardized to our negative control to calculate the fold change in β-hexosaminidase activity over background. C, Summary, showing the percent increase in β-hexosaminidase activity for K-RNT treatment compared with control for each level of IgE sensitization. Values are means ± SE ($n = 5$). Asterisk indicates significantly different values compared with control ($p < .05$, 2-way ANOVA followed by Sidak's *post hoc* comparison).

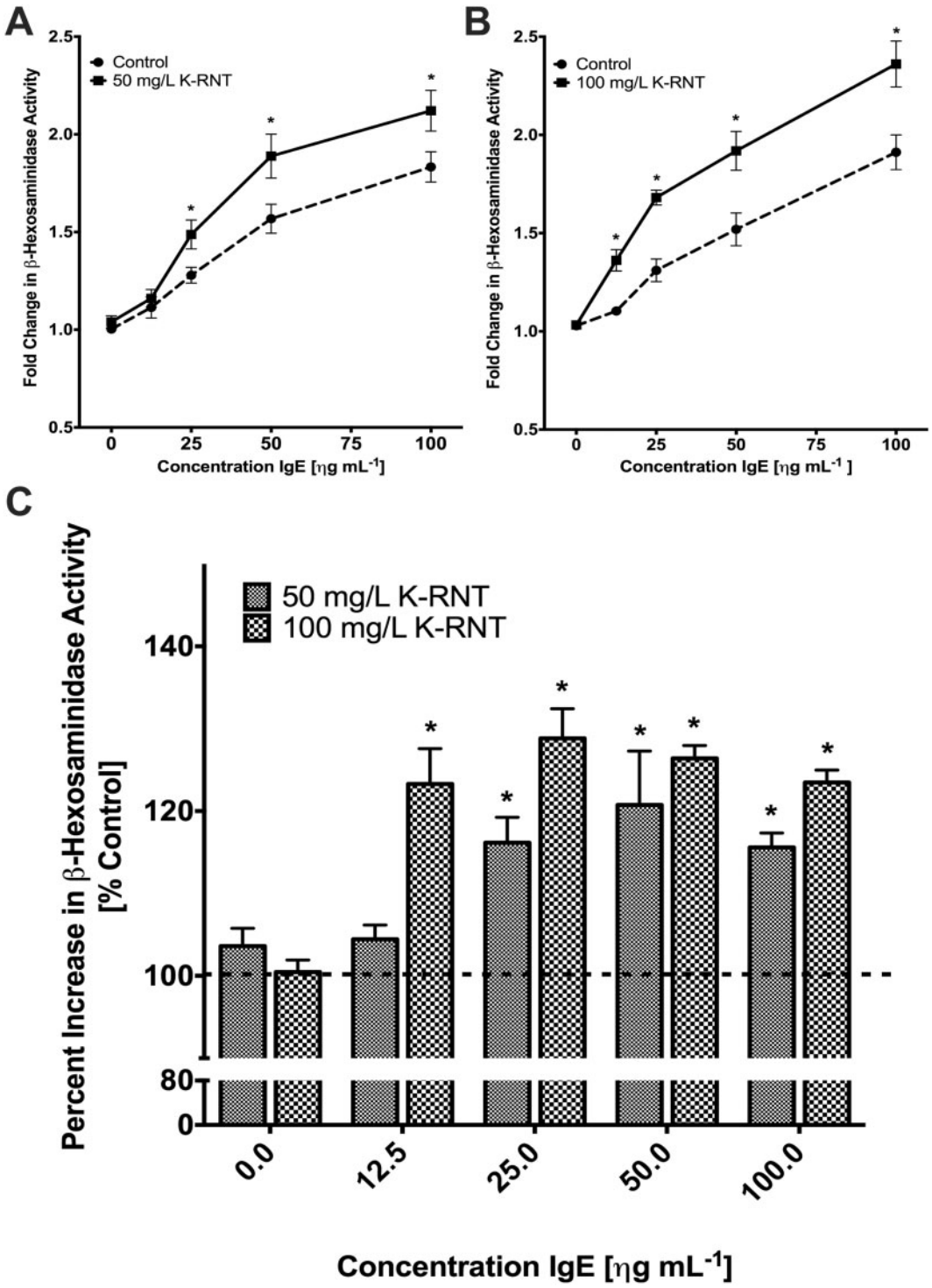

FIG. 5. RBL-2H3 cells showed increased degranulation after preexposure to K-RNTs. RBL-2H3 cells were seeded at 4×10^4 into a 96-well plate and allowed to rest for 2 h. Cells were then exposed to (A) 50 or (B) 100 mg l^{-1} K-RNT for 2 h. Cells were washed to remove K-RNTs before sensitization with 0, 12.5, 25, 50, or 100 ng ml^{-1}IgE and subsequent treatment with DNP-HSA to stimulate degranulation. Supernatant was collected and β-hexosaminidase activity assayed. The relative RFUs for each treatment was standardized to our negative control to calculate the fold change in β-hexosaminidase activity over background. C, Summary, showing the percent increase in β-hexosaminidase activity compared with control. Values are means ± SE ($n = 5$). Asterisk indicates significantly different values compared with control ($p < .05$, 2-way ANOVA followed by Sidak's *post hoc* comparison).

exposure to K-RNTs increased β-hexosaminidase release, with and without IgE sensitization (Fig. 4C) suggesting these materials can augment IgE-mediated release of granular products, but can also induce degranulation in RBL-2H3 cells independent of normal immune activating processes. Previous reports in Calu-3 pulmonary epithelial cells and U937 cells, a human macrophage cell line, demonstrated that exposure to 50 mg l^{-1} K-RNT for 1 and 6 h induced cytokine secretion (Journeay *et al.*, 2008).

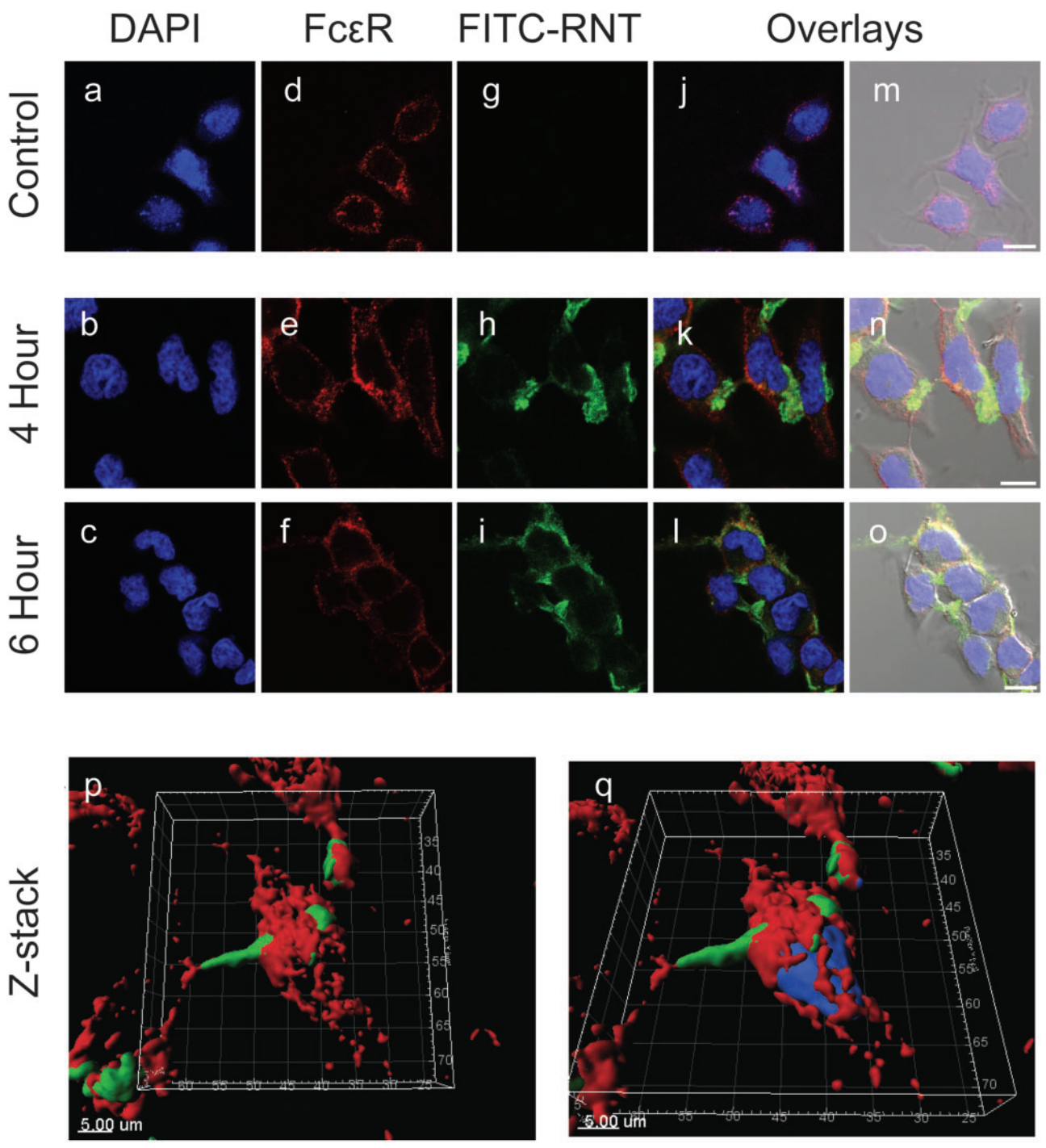

FIG. 6. Confocal micrographs showing association of FITC^{1}/TBL^{19}-RNTs with RBL-2H3 cells. Cells were stained for FCεR using IgE primary antibody and goat anti-mouse IgG PE-conjugated secondary antibody before being fixed. Nuclei were stained using DAPI. Laser scanning confocal micrographs with DAPI fluorescence (a, b, c), FCεR fluorescence (d, e, f), FITC-RNT fluorescence (g, h, i), fluorescence overlay (j, k, l), and bright-field overlay (m, *n*, o) of RBL-2H3 cells exposed to vehicle control for 4 h (top) or 10 mg l^{-1} FITC^{1}/TBL^{19} for 4 (middle) or 6 (bottom) h. Scale bars are 10 μm. Surface rendering and 3-dimensional (3D) reconstruction of Z-stack images suggest FITC-RNTs are internalized in RBL-2H3 cells after 2 h of exposure. (*p*, *q*) RBL-2H3 cells were exposed to 10 mg l^{-1} FITC^{1}/TBL^{19}-RNTs for 2 h and subsequently washed, stained for FCεR using IgE primary antibody and goat anti-mouse IgG PE-conjugated secondary antibody before being fixed. Nuclei were stained with DAPI. Surface rendering and 3D reconstruction of z-stack fluorescence was performed using Imaris software. FCεR fluorescence (red) and FITC^{1}/TBL^{19}-RNT fluorescence (green) shown without (*p*) and with (*q*) DAPI fluorescence (blue). Full color version available online.

Together these findings suggest K-RNTs may be proinflammatory, capable of eliciting an immune response through the earlier endpoints. Similar proinflammatory effects on mast cells have been reported for other high-aspect ratio NMs, including multi-wall carbon nanotube (Katwa *et al.*, 2012). RBL-2H3 cells have also been demonstrated to degranulate due to a variety of nonimmunological stimuli (Passante and Frankish, 2009). For example, Fowlkes *et al.* (2013) showed that mechanical loading in RBL-2H3 cells accomplished through RGD-binding integrin receptors caused secretion of β-hexosaminidase. With our

confocal results demonstrating a strong interaction with RBL-2H3 cell membranes, the observed increase in degranulation upon K-RNT exposure could be attributed to such physical stimulation.

To further investigate the proinflammatory response to K-RNTs, we tested the effect of preexposing RBL-2H3 to K-RNT on their ability to degranulate. In contrast to the previous experiment, residual unbound K-RNT was washed-off prior to sensitization with IgE. This step was essential to establish whether unbound K-RNTs were interfering with IgE binding its receptor, FcεRI. It is well known that many NMs nonspecifically bind to proteins in solution and thereby alter either their activity or affect their ability to bind to their cognate receptors (MacCormack *et al.*, 2012, Stueker *et al.*, 2014). Moreover, with confocal microscopy demonstrating a strong affiliation of K-RNTs with the cellular membrane, we wanted to determine if the noted effects were most likely due to K-RNTs remaining bound to the cells. We found that following 2 h preexposure to K-RNTs and subsequently washing away unbound K-RNT, cells were still able to elicit an IgE-mediated degranulatory response. However, unexpectedly, the cells demonstrated a significant increase in IgE mediated release of β-hexosaminidase compared with untreated cells.

To date, a variety of stimuli have been shown to induce degranulation in RBL-2H3 cells. It is possible that RNTs could be affecting membrane integrity in RBL-2H3 cells. Carbon NMs have been implicated in several studies to destabilize cellular membranes (Tahara *et al.*, 2012). If such a mechanism occurs in RBL-2H3 cells, the release of a variety of intracellular components, including β-hexosaminidase would result. However, because cells were washed prior to sensitization, we removed these factors and therefore suggest that K-RNTs are acting directly on the cell membrane and eliciting a potentiation of the IgE mediated degranulatory response. Our confocal microscopy demonstrated co-localization of RNTs with FcεRI. Therefore, it is possible RNTs potentiate the degranulatory response by increasing FcεRI cross-linking. Previous reports have suggested NMs can alter receptor cross-linking in RBL-2H3 cells, either promoting or inhibiting degranulation based largely on NM architecture. For example, gold nanoparticles larger than 19.8 nm, and coated with cell-activating antigens, promoted FcεRI cross-linking and activation and were potent effectors of RBL-2H3 degranulation; alternatively, antigen-coated gold NMs smaller than 19.8 nm competitively inhibited degranulation (Huang *et al.*, 2009). Interestingly, gold NMs alone did not elicit or alter a degranulatory response. RNTs are a high-aspect ratio NM with a diameter of 3.5 nm; however, they can be up to several 100-μm long. Given this large architecture, it is possible RNTs could be promoting FcεRI cross-linking and inducing degranulation in RBL-2H3 cells.

In conclusion, we have demonstrated that K-RNTs interact directly with the membrane of immune cells and can be internalized after exposure. These interactions affect viability and alter the ability of these cells to elicit receptor-mediated responses such as degranulation. In addition, at high doses, K-RNTs can elicit degranulatory responses irrespective of IgE mediated stimulation. Currently, we are trying to elucidate the nature of this interaction, the relative importance of membrane associated versus internalized K-RNTs, and the mechanism mediating this response. These questions are essential as we seek to understand the nature of the interactions between RNTs and cells and are important for tailoring RNTs for a variety of biomedical applications. For example, Fine *et al.* (2009) demonstrated that the biocompatibility of vascular stents could be improved with a 10 mg l^{-1} coating of K-RNTs, resulting in enhanced endothelial cell adherence. The utility of RNTs for such applications can be advanced by minimizing negative interactions with the immune system, ultimately improving biocompatibility.

SUPPLEMENTARY DATA

Supplementary data are available online at http://toxsci.oxfordjournals.org/.

FUNDING

This work was supported by the Natural Sciences and Engineering Research Council of Canada-National Research Council of Canada-Business Development Bank of Canada-Environment Canada (NSERC-NRC-BDC-EC Nanotechnology Initiative Grant Number NNBPJ 380151–08) and Alberta Innovates Technology Futures Nanoworks Grant (Grant Number PAB01015). J.D.E. was supported by an NSERC Vanier Canadian Graduate Scholarship and an Alberta Innovates Graduate Student Scholarship. V.A.O. is supported by NSERC Postgraduate Scholarship-Doctoral and the Alberta Innovates Health Solutions Graduate Studentship.

ACKNOWLEDGMENTS

The authors thank Biological Sciences Aquatic Facilities for all their help and assistance, Geraldine Barron at the Cross Cancer Cell Imaging Facility for her help with confocal microscopy and Dr Jon Veinot for advice and access to DLS analytical facilities.

REFERENCES

Borzsonyi, G., Beingessner, R. L., Yamazaki, T., Cho, J. Y., Myles, A. J., Malac, M., Egerton, R., Kawasaki, M., Ishizuka, K., Kovalenko, A., *et al.* (2010). Water-soluble J-type rosette nanotubes with giant molar ellipticity. *J. Am. Chem. Soc.* **132**, 15136–15139.

Braden, B. C., Goldbaum, F. A., Chen, B. X., Kirschner, A. N., Wilson, S. R., and Erlanger, B. F. (2000). X-ray crystal structure of an anti-Buckminsterfullerene antibody Fab fragment: Biomolecular recognition of C60. *Proc. Natl. Acad. Sci. U.S.A.* **97**, 12193–12197.

Chen, B. A., Jin, N., Wang, J., Ding, J., Gao, C., Cheng, J., Xia, G., Gao, F., Zhou, Y., Chen, Y., *et al.* (2010). The effect of magnetic nanoparticles of Fe_3O_4 on immune function in normal ICR mice. *Int. J. Nanomed.* **5**, 593–599.

Chen, B. X., Wilson, S. R., Das, M., Coughlin, D. J., and Erlanger, B. F. (1998). Antigenicity of fullerenes: Antibodies specific for fullerenes and their characteristics. *Proc. Natl. Acad. Sci. U.S.A.* **95**, 10809–10813.

Chhabra, R., Moralez, J. G., Raez, J., Yamazaki, T., Cho, J. Y., Myles, A. J., Kovalenko, A., and Fenniri, H. (2009). One-pot nucleation, growth, morphogenesis, and passivation of 1.4 nm Au nanoparticles on self-assembled rosette nanotubes. *J. Am. Chem. Soc.* **132**, 32–33.

Cortes, H. D., Lillico, D. M. E., Zwozdesky, M. A., Pemberton, J. G., O'Brien, A., Montgomery, B. C. S., Wiersma, L., Chang, J. P., and Stafford, J. L. (2014). Induction of phagocytosis and intracellular signaling by an inhibitory channel catfish leukocyte immune-type receptor: Evidence for immunoregulatory receptor functional plasticity in teleosts. *J. Innate Immun.* **6**, 435–455.

Cortes, H. D., Montgomery, B. C., Verheijen, K., García-García, E., and Stafford, J. L. (2012). Examination of the stimulatory signaling potential of a channel catfish leukocyte immune-type receptor and associated adaptor. *Dev. Comp. Immunol.* **36**, 62–73.

Fenniri, H., Deng, B. L., and Ribbe, A. E. (2002a). Helical rosette nanotubes with tunable chiroptical properties. *J. Am. Chem. Soc.* **124**, 11064–11072.

Fenniri, H., Deng, B. L., Ribbe, A. E., Hallenga, K., Jacob, J., and Thiyagarajan, P. (2002b). Entropically driven self-assembly of multichannel rosette nanotubes. *Proc. Natl. Acad. Sci. U.S.A.* **99**, 6487–6492.

Fenniri, H., Mathivanan, P., Vidale, K. L., Sherman, D. M., Hallenga, K., Wood, K. V., and Stowell, J. G. (2001). Helical rosette nanotubes: Design, self-assembly, and characterization. *J. Am. Chem. Soc.* **123**, 3854–3855.

Fine, E., Zhang, L., Fenniri, H., and Webster, T. J. (2009). Enhanced endothelial cell functions on rosette nanotube-coated titanium vascular stents. *Int. J. Nanomed.* **4**, 91–97.

Fowlkes, V., Wilson, C. G., Carver, W., and Goldsmith, E. C. (2013). Mechanical loading promotes mast cell degranulation via RGD-integrin dependent pathways. *J. Biomech.* **46**, 788–795.

Gilfillan, A. M., and Tkaczyk, C. (2006). Integrated signalling pathways for mast-cell activation. *Nat. Rev. Immunol.* **6**, 218–230.

Gustafsson, Å., Lindstedt, E., Elfsmark, L. S., and Bucht, A. (2011). Lung exposure of titanium dioxide nanoparticles induces innate immune activation and long-lasting lymphocyte response in the Dark Agouti rat. *J. Immunotoxicol.* **8**, 111–121.

Hamad, I., Al-Hanbali, O., Hunter, A. C., Rutt, K. J., Andresen, T. L., and Moghimi, S. M. (2010). Distinct polymer architecture mediates switching of complement activation pathways at the nanosphere–serum interface: Implications for stealth nanoparticle engineering. *ACS Nano* **4**, 6629–6638.

Huang, Y. F., Liu, H., Xiong, X., Chen, Y., and Tan, W. (2009). Nanoparticle-mediated IgE-receptor aggregation and signaling in RBL mast cells. *J. Am. Chem. Soc.* **131**, 17328–17334.

Journeay, W. S., Suri, S. S., Moralez, J. G., Fenniri, H., and Singh, B. (2008). Low inflammatory activation by self-assembling rosette nanotubes in human Calu-3 pulmonary epithelial cells. *Small* **4**, 817–823.

Journeay, W. S., Suri, S. S., Moralez, J. G., Fenniri, H., and Singh, B. (2009). Macrophage inflammatory response to self-assembling rosette nanotubes. *Small* **5**, 1446–1452.

Katwa, P., Wang, X., Urankar, R. N., Podila, R., Hilderbrand, S. C., Fick, R. B., Rao, A. M., Ke, P. C., Wingard, C. J., and Brown, J. M. (2012). A carbon nanotube toxicity paradigm driven by mast cells and the IL-33/ST2 axis. *Small* **8**, 2904–2912.

Kolosnjaj-Tabi, J., Hartman, K. B., Boudjemaa, S., Ananta, J. S., Morgant, G., Szwarc, H., Wilson, L. J., and Moussa, F. (2010). In vivo behavior of large doses of ultrashort and full-length single-walled carbon nanotubes after oral and intraperitoneal administration to swiss mice. *ACS Nano* **4**, 1481–1492.

Lin, J., Zhang, H., Chen, Z., and Zheng, Y. (2010). Penetration of lipid membranes by gold nanoparticles: Insights into cellular uptake, cytotoxicity, and their relationship. *ACS Nano* **4**, 5421–5429.

Maccormack, T. J., Clark, R. J., Dang, M. K. M., Ma, G., Kelly, J. A., Veinot, J. G. C., and Goss, G. G. (2012). Inhibition of enzyme activity by nanomaterials: Potential mechanisms and implications for nanotoxicity testing. *Nanotoxicology* **6**, 514–525.

Meng, J., Yang, M., Jia, F., Xu, Z., Kong, H., and Xu, H. (2011). Immune responses of BALB/c mice to subcutaneously injected multi-walled carbon nanotubes. *Nanotoxicology* **5**, 583–591.

Moralez, J. G., Raez, J., Yamazaki, T., Motkuri, R. K., Kovalenko, A., and Fenniri, H. (2005). Helical rosette nanotubes with tunable stability and hierarchy. *J. Am. Chem. Soc.* **127**, 8307–8309.

Ong, K. J., MacCormack, T. J., Clark, R. J., Ede, J. D., Ortega, V. A., Felix, L. C., Dang, M. K., Ma, G., Fenniri, H., Veinot, J. G., *et al.* (2014). Widespread nanoparticle-assay interference: Implications for nanotoxicity testing. *Plos One* **9**, 1–9.

Ortega, V. A., Katzenback, B. A., Stafford, J. L., Belosevic, M., and Goss, G. G. (2015). Effects of polymer-coated metal oxide nanoparticles on goldfish (Carassius auratus) neutrophil viability and function. *Nanotoxicology*. **9**, 23–33.

Passante, E., and Frankish, N. (2009). The RBL-2H3 cell line: Its provenance and suitability as a model for the mast cell. *Inflamm. Res.* **58**, 737–745.

Pfaller, T., Puntes, V., Casals, E., Duschl, A., and Oostingh, G. J. (2009). In vitro investigation of immunomodulatory effects caused by engineered inorganic nanoparticles – the impact of experimental design and cell choice. *Nanotoxicology* **3**, 46–59.

Rallo, R., France, B., Liu, R., Nair, S., George, S., Damoiseaux, R., Giralt, F., Nel, A., Bradley, K., and Cohen, Y. (2011). Self-organizing map analysis of toxicity-related cell signaling pathways for metal and metal oxide nanoparticles. *Environ. Sci. Technol.* **45**, 1695–1702.

Remes, A., and Williams, D. F. (1992). Immune response in biocompatibility. *Biomaterials* **13**, 731–743.

Ryan, J. J., Bateman, H. R., Stover, A., Gomez, G., Norton, S. K., Zhao, W., Schwartz, L. B., Lenk, R., and Kepley, C. L. (2007). Fullerene nanomaterials inhibit the allergic response. *J. Immunol.* **179**, 665–762.

Sim, R. B., and Wallis, R. (2011). Surface properties: Immune attack on nanoparticles. *Nat. Nanotechnol.* **6**, 80–81.

Song, S., Chen, Y., Yan, Z., Fenniri, H., and Webster, T. J. (2011). Self-assembled rosette nanotubes for incorporating hydrophobic drugs in physiological environments. *Int. J. Nanomed.* **6**, 101–107.

Song, Y., Li, X., and Du, X. (2009). Exposure to nanoparticles is related to pleural effusion, pulmonary fibrosis and granuloma. *Eur. Respir. J.* **34**, 559–567.

Stueker, O., Ortega, V. A., Goss, G. G., and Stepanova, M. (2014). Understanding Interactions of Functionalized Nanoparticles with Proteins: A Case Study on Lactate Dehydrogenase. *Small* **10**, 2006–2021.

Sun, L., and Wang, X. (2014). A new kind of cell suicide: Mechanisms and functions of programmed necrosis. *Trends Biochem. Sci.* **39**, 587–593.

Sun, L., Zhang, L., Hemraz, U. D., Fenniri, H., and Webster, T. J. (2012). Bioactive rosette nanotube-hydroxyapatite nanocomposites improve osteoblast functions. *Tissue Eng., Part A* **18**, 1741–1750.

Tan, F., Wang, M., Wang, W., and Lu, Y. (2008). Comparative evaluation of the cytotoxicity sensitivity of six fish cell lines to four heavy metals in vitro. *Toxicol. in vitro* **22**, 164–170.

Tahara, Y., Nakamura, M., Yang, M., Zhang, M., Iijima, S., and Yudasaka, M. (2012). Lysosomal membrane destabilization induced by high accumulation of single-walled carbon nanohorns in murine macrophage RAW 264.7. *Biomaterials* **33**, 2762–2769.

Tikhomirov, G., Oderinde, M., Makeiff, D., Mansouri, A., Lu, W., Heirtzler, F., Kingsley, S., Kwok, D. Y., and Fenniri, H. (2008). Synthesis of hydrophobic derivatives of the G/\C base for rosette nanotube self-assembly in apolar media. *J. Org. Chem.* **73**, 4248–4251.

Zhao, X., Ong, K. J., Ede, J. D., Stafford, J. L., Ng, K. W., Goss, G. G., and Loo, S. C. J. (2013). Evaluating the toxicity of hydroxyapatite nanoparticles in catfish cells and zebrafish embryos. *Small* **9**, 1734–1741.